Received: 22 February 2021 | Revised: 4 October 2021 | Accepted: 24 November 2021

DOI: 10.1002/mp.15403

RESEARCH ARTICLE

MEDICAL PHYSICS

# Commissioning of carbon-ion radiotherapy for moving targets at the Osaka Heavy-Ion Therapy Center

**Noriaki Hamatani**[1] | **Toshiro Tsubouchi**[1] | **Masaaki Takashina**[1] | **Masashi Yagi**[2] | **Tatsuaki Kanai**[1]

[1] Osaka Heavy-Ion Therapy Center, Osaka, Japan

[2] Department of Carbon Ion Radiotherapy, Osaka University Graduate School of Medicine, Osaka, Japan

**Correspondence**
Noriaki Hamatani, Osaka Heavy-Ion Therapy Center, 3-1-10, Otemae, Chuo-ku, Osaka 540-0008, Japan.
Email: n.hamatani@osaka-himak.or.jp

**Funding information**
JSPS KAKENHI, Grant Number JP17H04119

## Abstract

**Purpose:** Herein, we report the methods and results of the Hitachi carbon-ion therapy facility commissioning to determine the optimum values of the magnitude of movement and repaint number in respiratory-gated irradiation.

**Methods:** A virtual-cylinder target was created using the treatment-planning system (VQA Plan), and measurements were performed to study the effects of respiratory movements using a two-dimensional ionization-chamber array detector and a phantom with movable wedge and stage. For simulations, we selected a $10 \times 10 \times 10$ cm$^3$ cubic irradiation pattern with a uniform physical dose and two actual cases of liver-cancer treatments, whose prescribed doses were 60 Gy(RBE)/4 fraction (Case 1) and 60 Gy(RBE)/12 fraction (Case 2). We employed two types of repainting methods, one produced by the algorithm of VQA Plan (VQA algorithm) and the other by ideal repainting. The latter completely repeats all spots with set number of repaintings. We performed flatness calculations and gamma analysis to evaluate the effects of each condition.

**Results:** From the measurements, the gamma passing rates for which the criteria were 3%/3 mm exceeded 95% for displacements in the head-to-tail direction if the repaint number was greater than 3 and the magnitude of the residual motions was less than 5.0 mm. In simulations with the cubic irradiation pattern, the gamma passing rates (with criteria of 2%/2 mm) exceeded 95% when the magnitude of the residual motions was 3.0 mm and the repaint number was greater than 3. When the repaint number was set to 4 in the VQA with the actual liver cases, the flatness results for Case 2 was minimal. For ideal repainting, the flatness results for all ports fell within ∼3.0% even when the magnitude of the residual motions was 5.0 mm if the repaint number was 6. However, the flatness was less than 3.0% for almost all ports if the magnitude of the residual motions was less than 3.0 mm with a repaint number of 4 in case of both types of repaint methods.

**Conclusions:** At our facility, carbon-ion radiotherapy can be provided safely to a moving target with residual motions of 3.0 mm magnitude and with a repaint number of 4.

**KEYWORDS**
carbon-ion radiotherapy, repaint, respiratory gating

## 1 | INTRODUCTION

Charged-particle beams can create particular dose distributions, known as Bragg peaks; therefore, they can produce dose distribution superior to those of photon beams. In particular, heavy ions have a narrow penumbra and a high biological effect around the Bragg peak,[1] and patients have been treated efficiently using these features.

At the Osaka Heavy-Ion Therapy Center (Osaka-HIMAK), carbon-ion radiotherapy (CIRT) began in October 2018. Our facility has adopted a hybrid energy-scanning method[2] that uses 12 accelerated energies between 100.0 and 430.0 MeV/u and range shifters. A combination of 12 types of accelerated energies and 7 types of range shifters can be used to create the 3.0-mm pitch layer. The facility uses the raster-scanning method, in which beam irradiation is not stopped during the movement from one spot to another. This differs from proton therapy's spot-scanning method, which allows fast scanning that saves irradiation time.

About 1 month after starting CIRT, we began the treatment of moving tumors, such as liver and lung cancers. In the scanned particle therapy, the relative motion between the target and the scanning beam has a substantial impact on the delivered dose.[3] It is known that scanning irradiation is less robust to organ motions than passive beam irradiation, owing to the interplay between the motions of the scanning beam and the motion of the tumor.[4] The interplay between target and beam motions usually causes hot and cold spots in the delivered dose distributions.[3,5] A number of methods have been proposed to resolve these problems, including respiratory gating, tracking,[6,7] and rescanning.[8,9] The respiratory-gated carbon-ion scanning radiotherapy to obtain the motion of surface has been commissioned in advance by National Institute of Radiological Science (Chiba, Japan),[10] and the facilities in Japan have adopted a similar system. Our facility adopted Anzai respiratory-gating system (Anzai Medical Co., Japan), real-time-image gated-particle therapy (RGPT) system,[11] and rescanning (herein referred as "repainting"). Although the details of the RGPT are beyond the scope of this paper because it is different from the respiratory-gating system and contains some unique features such as marker tracking with fluoroscopic X-ray images and the verification of exposure dose, it is essentially a respiratory-gating system and the commissioning results for the RGPT system will be reported separately.

To improve the robustness for scanning irradiation against moving targets, several other methods—such as phase-controlled rescanning (PCR) with fast scanning[8,12]—have been developed. Fast scanning is important to obtain acceptable irradiation times with a large number of rescans.[8] The PCR technique has been shown to improve dose conformation for lung tumors.[13] Moreover, dose conformation did not show a particular degradation with 8 × PCR, even when the irradiation respiratory cycle was changed from the planned respiratory cycle.[14] However, our facility does not have the PCR technique. Further, the rescanning method used in the treatment-planning system (VQA Plan ver. 5.8.1, Hitachi Ltd., Japan) is different from that of other CIRT facilities; although these facilities use roundtrip rescanning,[14] the VQA algorithm uses a one-way scanning direction for the repainting method. At the German cancer research center (DKFZ) facility, an extracranial stereotactic setup was developed to reduce the liver's intracorporal movement for single-dose radiation therapy.[15] In addition to rescanning and the respiratory-gating technique, abdomen compression was used at the Italian National Centre for Oncologic Hadrontherapy (CNAO) to reduce organ motion.[16] However, our facility does not use abdomen compressions.

To start the treatment with moving targets, an appropriate number of repaintings and the allowed target-motion distance inside a gating window (i.e., the magnitude of the residual motions) had to be determined. Although the AAPM Task Group 76 (TG-76) recommended the magnitude of motion,[17] center-specific criteria for motion target need to be established according to the specific technical properties of each delivery system.[18,19] To determine the criteria—the appropriate number of repaintings and the magnitude of the residual motions—we first performed measurements to investigate the effects of respiratory movements using a two-dimensional (2D) ionization-chamber array and a phantom (Figure 1a,b). We evaluated the measurement results only for the physical dose, and the measurement conditions were limited due to time constraints. Therefore, we performed simulations based on actual liver cases to assess the conditions for the treatment of moving targets specified clinical doses. Based on these findings, we report the determination of treatment conditions in this work. Additionally, because some anticipated improvement points were discovered, considerable solution will be stated in the discussion section.

## 2 | MATERIALS AND METHODS

### 2.1 | Main performance equipment and limitations

As stated in the Introduction section, our facility adapted the hybrid energy-scanning method with synchrotron. Although a strict 4D evaluation was not performed in our study, 4D parameters like energy switching time and dose rate are important factors for 4D treatment planning.[20] Furthermore, as mentioned in the discussion section, the limitation of the minimum monitor unit per spot (MU/spot) has an effect on the repainting. Table 1 shows a summary of the machine's performance and limitations.

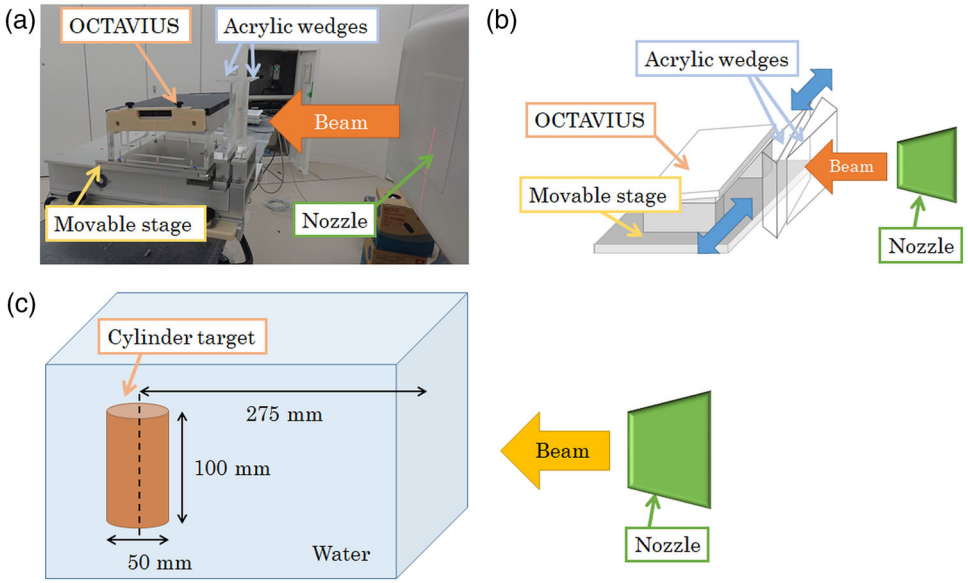


**FIGURE 1** (a) Photograph and (b) schematic of the measurement setup. The beam is irradiated from the right side, and the deep direction corresponds to the craniocaudal direction in the photograph. (c) Schematic of the virtual-cylinder target. The prescription dose was set to 430 cGy(RBE)/1 fraction

**TABLE 1** Summary of equipment performance and limitations

| Item | Value |
|---|---|
| Range of dose rate | From 1.0 to 8.0 MU/s for all energies |
| Minimum MU/spot | 0.0016 |
| Energy switching time | 0.5 s |
| Acceleration and deceleration time | 2.0 s |
| Scanning speed | 100.0 m/s in craniocaudal direction<br>50.0 m/s in another direction |
| Accumulated charge | 3.8 nC |

*Abbreviation*: MU, monitor unit.

## 2.2 | Measurement and analysis conditions

We performed commissioning based on measurements obtained using a 2D ionization-chamber array detector (OCTAVIUS detector 1500XDR, PTW, Freiburg, Germany), a phantom (investigating respiratory movements effects), AKMP02 (Accelerator Engineering Corporation, Japan), and a horizontal port for the radiation source. The phantom was equipped with two acrylic wedges, one of which could move toward left or right in a direction perpendicular to the beam and water-equivalent thickness could be altered during irradiation. Moreover, the phantom featured a movable stage that could be equipped with a 2D ionization-chamber array detector, whose position could be altered parallel to the scanning direction during irradiation. By tilting the detector's face downward (5.0°), the dose distribution in the depth direction could be obtained in one measurement (see Figure 1a,b). As the respiratory-gating system, laser sensor type AZ-733VI (Anzai Medical Co., LTD) was adopted in our facility. It can detect the motion of the surface with the measurement of the laser's reflection. The wave data was obtained by irradiating the moving target with laser. A virtual-cylindrical target in the water was created using the algorithm of VQA Plan (VQA algorithm) (radius = 25 mm, height = 100 mm, maximum range = 300 mm, and prescribed dose = 430 cGy(RBE)/1 fraction (fx); Figure 1c). The single-field uniform dose (SFUD) optimization method was used in this study. The numbers of repaintings were set to 1, 3, 4, and 6. The movement pattern followed was $f(x) = sin^4(x)$. The respiration cycle was set to 4.0 s, which is a typical respiration cycle.[21] The residual-motion magnitudes were set to 2.0 and 3.0 mm in the depth direction (i.e., using the movable wedge) and 2.0, 3.0, 5.0, 7.0, and 8.0 mm in the beam-scanning direction (using the movable stage). Separate measurements were obtained using the movable wedge and movable stage. As shown in the results section, deviations in the depth direction have minimal influence on the 2D gamma analysis[22] result; therefore, we primarily focused on the variation of displacements in the scanning direction. To save time, we repeated the measurements for each condition two or three times.

We performed 2D gamma analysis[22] using VeriSoft 7.1 software (PTW, Freiburg, Germany). The criteria were set to 3%/3 mm, and the threshold was set to 40% to exclude the penumbra region. Additionally, we performed measurements of the dose distribution without

any movement of the movable wedge and stage for use as the reference dose distribution.

## 2.3 | Simulation method

Because the respiratory-gating system at Osaka-HIMAK does not use the PCR technique, the carbon-ion beam is delivered to the target regardless of the respiration cycle or the accumulated charge remaining in the synchrotron while the gating window is open. Tumor motions can be considered as spot-position deviations that follow the probability-density function for tumor motion when the gating window is open. Therefore, for this study we generated the deviated spot-position data, and we used it to calculate dose distributions.

The spot-position deviations were created for two types of distributions. One type compromised uniform random values within a maximum value, which was changed from 1.0 to 5.0 mm with 1.0 mm steps. The other type of distribution followed a sine-wave probability-density function, which was a more strict condition than the function $f(x) = sin^4(x)$ adopted for the measurements. The sine-wave amplitude was fixed at 10.0 mm, and the gating levels were set between 10% and 50% with 10% steps; that is, the residual-motion magnitudes were set between 1.0 and 5.0 mm with 1.0 mm steps. Additionally, we fixed the movement cycle at 4.0 s. During irradiation, the respiration cycles and amplitudes of actual patients are not uniform.[14,23] Moreover, it has been reported that dose uniformity exhibits little response to changes in the respiration frequency.[9] Using a gating system, the magnitude of the residual motion was fixed within the gating window range. Therefore, it is expected that changes in the respiration cycle and amplitude can be ignored, and these parameters were fixed in this study. The deviation histograms were created and they were fitted by the following function.

$$f(x) = \frac{a}{\sqrt{x+b}} + c \quad (1)$$

Here, *a, b,* and *c* are the fitting parameters. Figure 2a shows an example of a sine wave with a gating level, a deviation histogram, and the fitting result is shown in Figure 2b when the gating level was set to 30%.

We used five trials in the simulations for both types of distributions.

## 2.4 | Repainting methods from the VQA plan and ideal conditions

We set the repainting number as 1, 2, 3, 4, and 6 for this simulation study. However, there are some limitations of the treatment machine used for the irradiation, that is, the minimum MU/spot is 0.0016 MU as presented in Table 1. The separation of each spot is decided using the repainting method employed in the VQA Plan once the decision of each MU/spot is obtained via optimization. The repainting numbers for some spots are forced to change to 1 if the MU/spot values divided by the repainting number are less than the minimum MU/spot; that is, these spots are subsequently deleted from each painting after the first painting. Consequently, the number of long spot intervals derived from the VQA algorithm increases with an increase in the number of repaintings. Therefore, in this study we performed simulations for the irradiation patterns obtained from the VQA algorithm and the ideal irradiation patterns. The latter ignored the limitation of the treatment machine; all the spots were completely repeated with the repainting number set by the treatment planner (ideal repainting).

**TABLE 2** Each item for the actual liver cases and simulation conditions

| Item | Case 1 | Case 2 |
|---|---|---|
| Prescribed dose | 60 Gy(RBE)[a]/4 fx | 60 Gy(RBE)/12 fx |
| Port angle | Vertical and horizontal | |
| Repainting algorithm in simulation | VQA algorithm[b] and ideal[c] | |
| Number of repaintings | 1, 2, 3, 4, 6 | |
| Magnitude of residual motion | From 1.0 to 5.0 mm in 1.0 mm steps | |

*Abbreviations*: fx, fraction; RBE, relative biological effectiveness.
[a]Clinical dose.
[b]The algorithm adopted by the treatment-planning system (VQA Plan ver. 5.8.1, Hitachi Ltd., Japan).
[c]All spots are completely repeated with the repainting number set by the treatment planner.

## 2.5 | Simple irradiation pattern

For the simple irradiation pattern, we selected a cubic irradiation pattern. Its field size was 10 × 10 $cm^2$, and the length of the spread-out Bragg peak (SOBP) was 10 cm—ranging from 10 to 20 cm depth in water—which is a uniform physical dose and is the reference field for our facility. The spot spacing was 3.0 mm, and the physical dose was 200.0 cGy in the SOBP region.

This irradiation pattern was created without using the VQA Plan. The original pattern involved only one painting, and the limitation due to the minimum MU/spot was ignored for any repainting cases.

## 2.6 | The actual plans for two liver cases

Two liver cases treated at Osaka-HIMAK were selected. Information about each case and the simulation conditions are presented in Table 2. Both plans were created using the SFUD optimization method. For Case 1, both

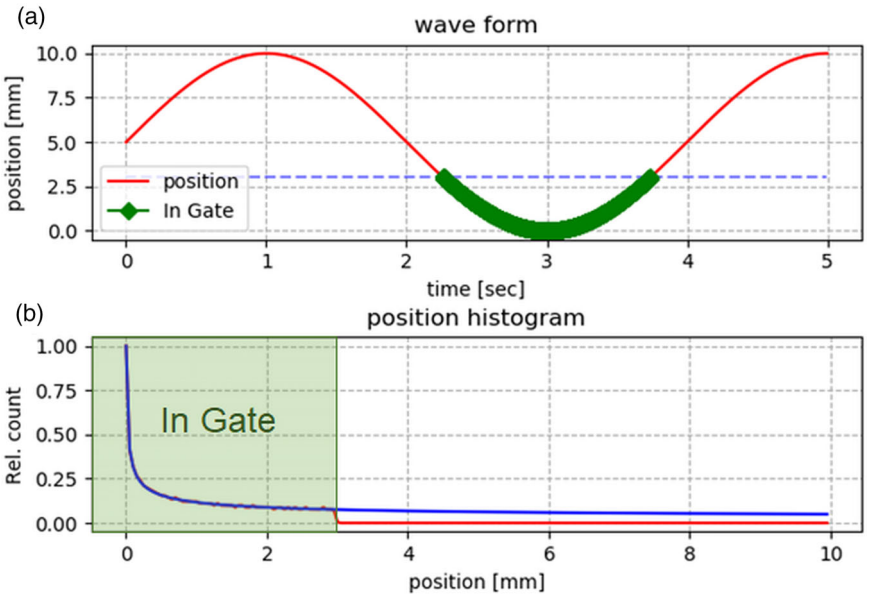


**FIGURE 2** (a) Sine wave with 10.0-mm amplitude (red solid line), 30% gating level (blue dashed line), and positions in which the gating window is open (green line dots). (b) Normalized histogram of positions with the open gating window (red solid line) and the results from the fitting function given by Equation (1) (blue solid line). The green painted area corresponds to the region with open gating window

vertical and horizontal ports are irradiated per day, while the one port is irradiated per day in Case 2.

For Cases 1 and 2, we performed simulations for both the irradiation patterns planned using the VQA algorithm and those obtained with the ideal repainting method. Using the VQA patterns, we ran optimization with each repainting number under identical conditions as for the clinically approved plan. Using ideal repainting, however, we created plans with the repainting number set to 1, and exported the irradiation-spot file. Then, we divided the MU for each spot equally among the given number of repaintings using in-house software.

For creating the deviations for the simulations, we adopted only the distribution following the probability-density function; because the results for the simple irradiation pattern were almost independent of the types of deviation distributions, as shown in the results section.

## 2.7 | Analysis method for the simulations

For the simple irradiation pattern, we performed 3D gamma analysis[22] and calculated its flatness. We calculated the gamma passing rates using VeriSoft software, with the criteria of gamma analysis set to 3%/3 mm, 2%/2 mm, and 1%/1 mm. We calculated the flatness using the following equation[24]:

$$\text{Flatness} = \frac{D_{\max} - D_{\min}}{D_{\max} + D_{\min}} \times 100, \qquad (2)$$

where $D_{\max}$ and $D_{\min}$ are the maximum and minimum doses, respectively, in the analysis region.

For the simple irradiation pattern, we set the region used for evaluating the flatness to be 70% of the SOBP region, and we calculated the flatness using the physical dose distribution. For the actual liver cases, we calculated the flatness within the clinical target volume (CTV) using Equation (2) with the clinical dose.

The summary of the items for the experiment and the simulation conditions are presented in Table 3.

## 2.8 | Statistical analysis

We used *t*-test to evaluate the relationship between the repainting method obtained using the VQA algorithm and ideal repainting. The boundary for judging whether there was a considerable difference was set to 5.0% (0.05).

# 3 | RESULTS

## 3.1 | Measurements

Figure 3 shows the measurement results for the 2D gamma passing rate plotted against the magnitude of the residual motion. The points on the graph represent the average values, while the error bars indicate the standard deviations (one sigma). The gamma passing rates for the depth-direction deviations exceeded 95% in all the cases (Figure 3a). For the scanning-direction displacements, the gamma passing rates exceeded 95%, including error bars, when the magnitude of the residual motion was less than 5.0 mm and the repainting numbers were greater than 3 (Figure 3b).

**TABLE 3** Summary of experimental and simulations conditions

| Contents | Experiment | Simulation |
|---|---|---|
| Target type | Cylindrical target[a] | Square target[b]Two liver cases (4 ports in total) |
| Magnitude of residual motion | Depth direction: 2 and 3 mmCranio-caudal direction: 2, 3, 5, 7, and 8 mm | Craniocaudal direction: 1, 2, 3, 4, and 5 mm |
| Dose type for evaluation | Physical dose | Physical dose (square target)Clinical dose (liver cases) |
| Motion pattern | $\sin^4(x)$ | $\sin(x)$ |
| Repainting number | 1, 3, 4, and 6 | 1, 2, 3, 4, and 6 |
| Repainting method | VQA algorithm[c] | Only ideal method[d] (square target)VQA algorithm and ideal method (liver cases) |

[a]Dummy target with radius = 25 mm; height = 100 mm.
[b]$10 \times 10 \times 10$ cm$^3$ with the maximum range 20 cm.
[c]The algorithm adopted by the treatment-planning system (VQA Plan ver. 5.8.1, Hitachi Ltd., Japan). When the monitor unit (MU) values of some spots divided by the repainting number become smaller than the limit of minimum MU, the number of repainting of those spots is changed to 1.
[d]All spots are repeated completely with the repainting number set by planners.

## 3.2 | Simulations using the simple irradiation pattern

Figure 4 shows the flatness calculations for the simulation results of the simple irradiation pattern against the magnitudes of the residual motions (Figure 4a) and the number of repaintings (Figure 4b). The points on the graphs represent the averaged values of flatness, while the error bars represent the standard deviations. The solid lines with circles indicate the results for uniform random residual motions, while the dashed lines with triangles represent the results for residual-motion distributions that follow the sine-wave probability-density function. The results of flatness computation improved as the number of repaintings were increased. When the magnitude of the residual motion following the probability-density function was set to 5.0 mm, the flatness became 8.60% ± 0.27% for a repainting number 1 and 4.30% ± 0.48% for a repainting number 6. The flatness results improved by ∼3.0% if the magnitude of the residual motions was less than 2.0 mm.

Notably, these results had almost no dependence on the nature of the residual-motion distribution. We performed a *t*-test for the flatness results, comparing uniform random residual motions with the motions that followed the probability-density function for each magnitude of residual motions and each repainting number. There was insignificant difference in the flatness between these two types of motions, except for the case where the repainting number was 1, with a 4 mm magnitude of residual motion ($p < 0.04$).

Figure 5 shows the results of the passing rates from 3D gamma analysis, depending on the magnitudes of the residual motions. The solid lines with circles indicate the results for uniform random residual motions, and the dashed lines with triangles indicate the results for the probability-density function residual motions. The points on the graph indicate the averaged values, and the error bars represent the standard deviations. For the flatness calculations, the gamma passing rates improved as the number of repaintings increased. When the criteria of gamma analysis were set to 3%/3 mm, the results exceeded 90% for all magnitudes of residual motions if the number of repaintings was more than 2. When the criteria were set to 2%/2 mm and the magnitude of

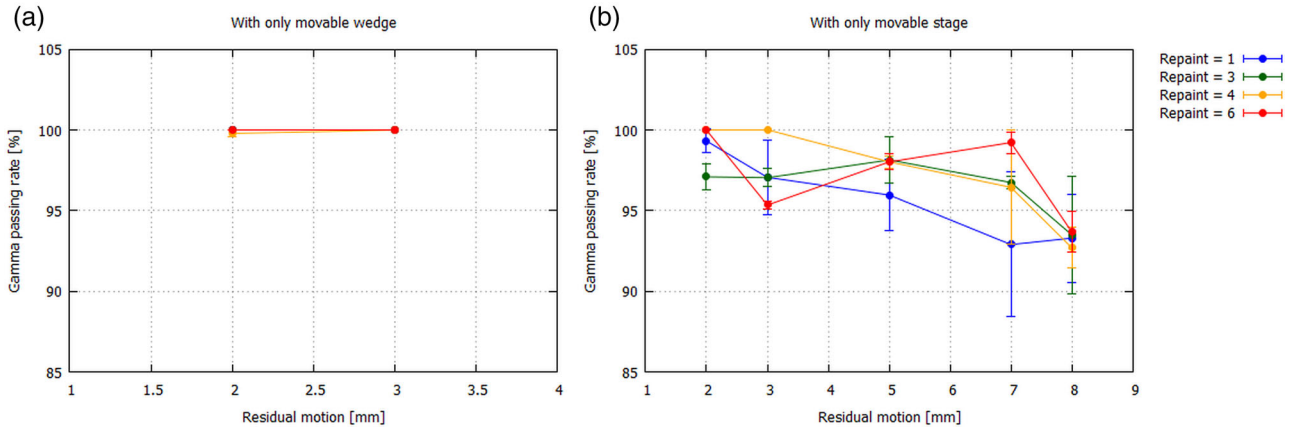


**FIGURE 3** Gamma analysis results with the gamma passing rate plotted against the magnitude of residual motions. The criteria were set to 3%/3 mm, and each solid line point indicates the result with each repainting number (Repaint = 1, 3, 4, and 6). The error bars mean the standard deviations. (a) The resulting gamma passing rates for residual motions in the depth direction only by the movable wedge. (b) The resulting gamma passing rates for residual motions in the beam-scanning direction only by the movable stage

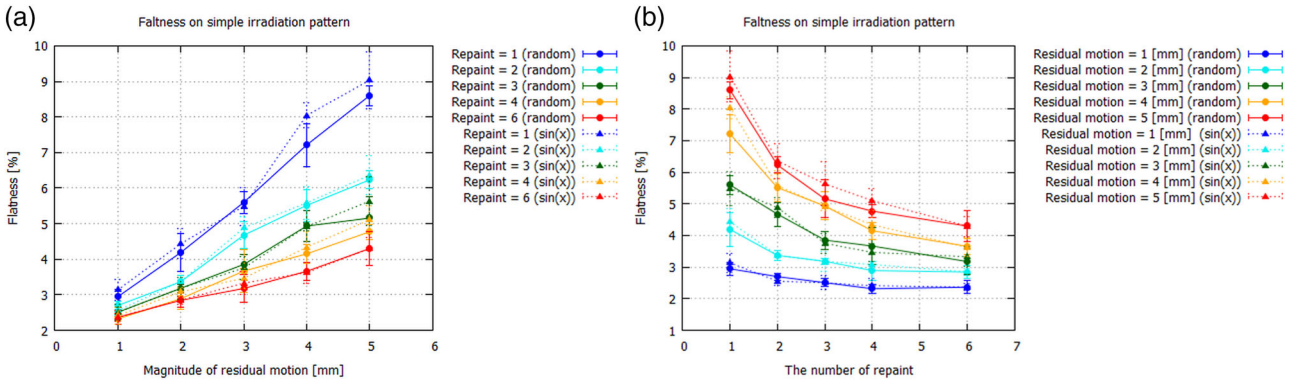


**FIGURE 4** Flatness calculation results for the simulation using the simple irradiation pattern ($10 \times 10 \times 10$ cm$^3$ field). The solid lines with circles indicate the results with the uniform random magnitude of residual motion (random), and the dashed lines with triangles indicate the results with the magnitudes of residual motion following probability-density function derived from sine function (sin($x$)). Error bars indicate the standard deviation. Flatness against the (a) magnitude of the residual motions and (b) number of repaintings

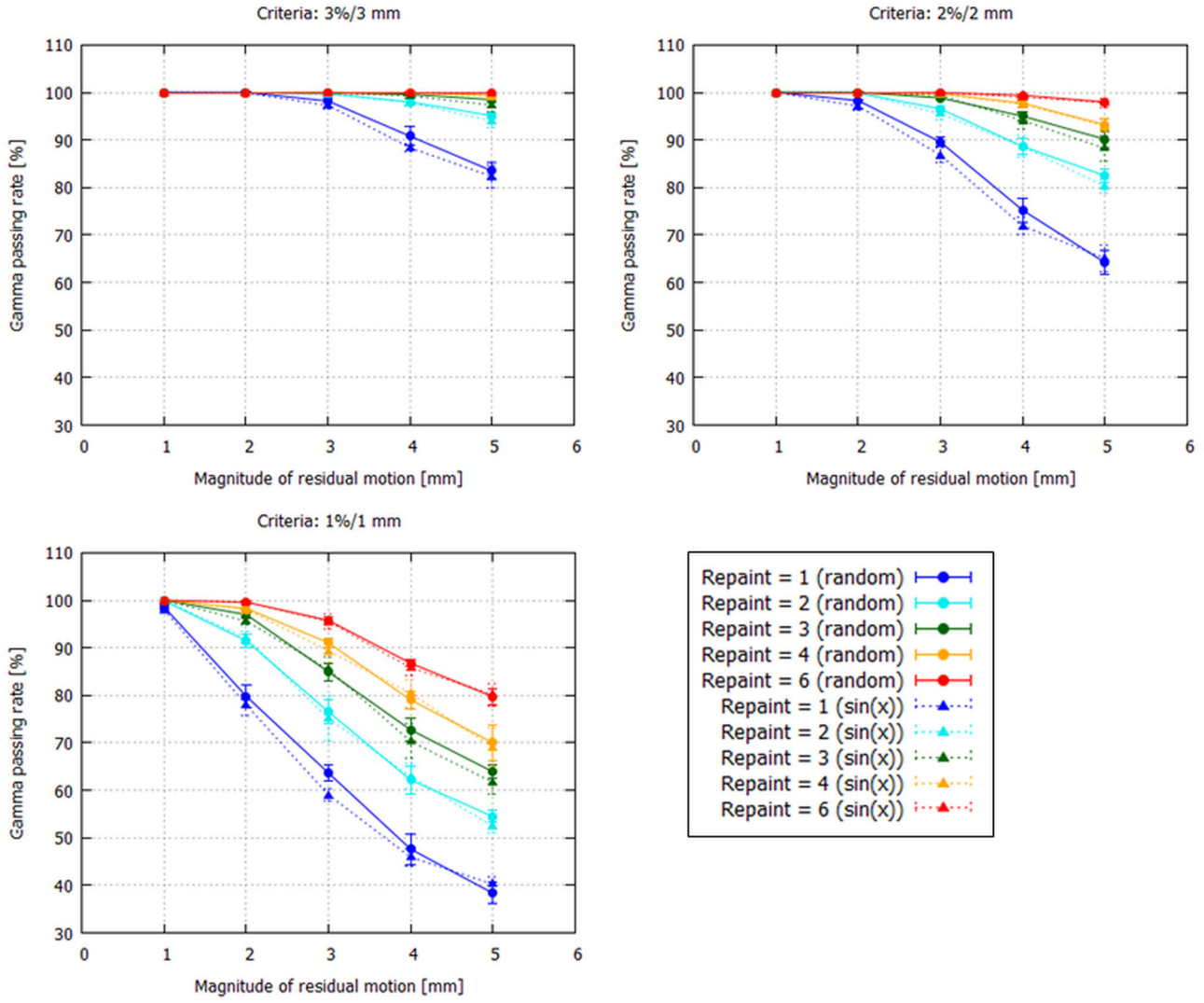


**FIGURE 5** Three-dimensional gamma analysis results; gamma passing rates against the magnitude of residual motion, with the simple irradiation pattern ($10 \times 10 \times 10$ cm$^3$ field). The criteria were (a) 3%/3 mm, (b) 2%/2 mm, and (c) 1%/1 mm. The analysis region was set to 70% of the field size. The solid lines with circles indicate the results with the uniform random magnitude of residual motion (random). The dashed lines with triangles indicate the results with the magnitudes of residual motion following the probability-density function (sin($x$)). Standard deviations are shown by error bars. Different colors indicate the types of repainting numbers (Repaint = 1, 2, 3, 4, and 6)

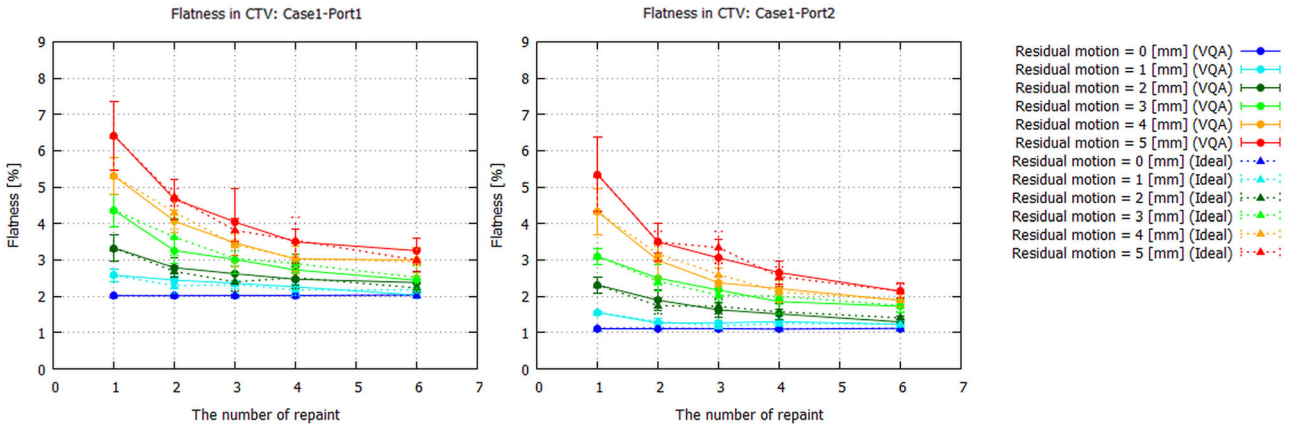


**FIGURE 6** Flatness calculation results in CTV against the repaint numbers for liver Case 1 (prescription dose was 60 Gy(RBE)/4 fx). Results for (a) port 1 and (b) port 2. Each colored line represents the type of the magnitude of residual motion (Residual motion = 0, 1, 2, 3, 4, and 5 mm). The solid lines with circles show the results using VQA repainting method created by the treatment-planning system (VQA). The dashed lines with triangle indicate the results using the ideal repainting method, all spots completely repeated (ideal); error bars indicate the standard deviation

the residual motion was 3.0 mm, the gamma passing rates exceeded 95%, including the width of the error bar, when the number of repaintings was more than 3. When the number of repaintings was set to 6, the average gamma passing rates exceeded 95% even when the criteria were 1%/1 mm with 3.0 mm residual motions. Further, the gamma passing rates had little dependence on the types of distributions of the magnitude of residual motions. We conducted a *t*-test for the gamma passing rate results, as for the flatness calculations. Although there were significant differences in the cases with the criteria of 2%/2 mm and 1%/1 mm when the number of repaintings was 1 with 3.0 mm residual motions ($p < 0.02$ and $p < 0.004$, respectively), there was insignificant difference on the cases with other conditions.

## 3.3 | Simulations with the actual plans for the liver cases

We performed simulations of respiratory-gated CIRT using the actual treatment plans for two liver cases. When the simple irradiation pattern was used, the type of distribution of the magnitude of residual motions had negligible effect on the results of the flatness calculation or the 3D gamma analysis. Therefore, we only used the residual-motion distribution that followed the probability-density function for the actual treatment plans. In addition, we used two types of repainting methods: one derived from the VQA algorithm and the other from ideal repainting. Figure 6 shows the resulting flatness within the CTV for Case 1, where the prescribed dose was 60 Gy(RBE)/4 fx. The points on the graph show the averaged values of the flatness calculations, and the error bars represent the standard deviations. The solid lines with circles represent the results obtained using the VQA repainting, and the dashed lines with triangles indicate the results obtained with the ideal repainting method. The flatness improved as the number of repaintings increased. When the magnitude of the residual motion was 5.0 mm, the resulting flatness with one painting on port 1 of Case 1 was 6.42% ± 0.94% and the flatness results for six paintings were 3.26% ± 0.35% using the VQA repainting and 3.00% ± 0.32% with ideal repainting. There was almost no difference due to the different repainting methods.

Figure 7 shows the resulting flatness in the CTV for Case 2, for which the prescribed dose was 60 Gy(RBE)/12 fx. When the ideal repainting method was adopted, the flatness results improved as the number of repaintings increased. However, for the repaint obtained using the VQA algorithm, the resulting flatness became worse when the number of repaintings increased above 4. When the number of repaintings was set to 6, the flatness averages had minimum values for all the cases using ideal repainting. However, if the size of the residual vibrations was less than 3.0 mm, the difference in the flatness for different numbers of repaintings was not particularly high.

Figure 8a depicts the flatness results for all the cases with residual motions of 4.0 mm. For Case 2, the flatness averages obtained when using the VQA algorithm had minimal values for both the ports when the number of repaintings was set to 4 (3.21% ± 0.26% and 3.55% ± 0.24%), but they became worse when the number of repaintings was set to 6 (3.55% ± 0.36% and 4.16% ± 0.32%). Figure 8b shows the relation between the number of repaintings and the total number of spots for both repainting methods. For both the ports, the relation of Case 2 with the VQA repainting algorithm deviated considerably from linearity.

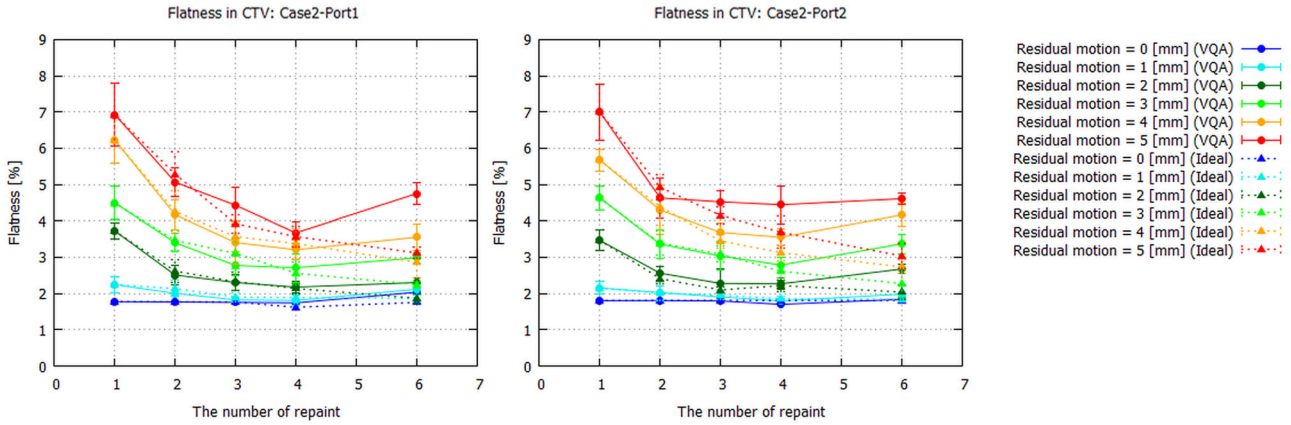


**FIGURE 7** Flatness results in CTV for liver Case 2 (prescription dose was 60 Gy(RBE)/12 fx) against the number of repaint. Results for (a) port 1 and (b) port 2. Each colored line color indicates the type of the magnitude of residual motion (Residual motion = 0, 1, 2, 3, 4, and 5 mm). The solid lines with circles indicate the results using the repainting method of the treatment-planning system (VQA). The dashed lines with triangle indicate the results using the repainting method that completely repeat all spots (ideal). Error bars indicate the standard deviation

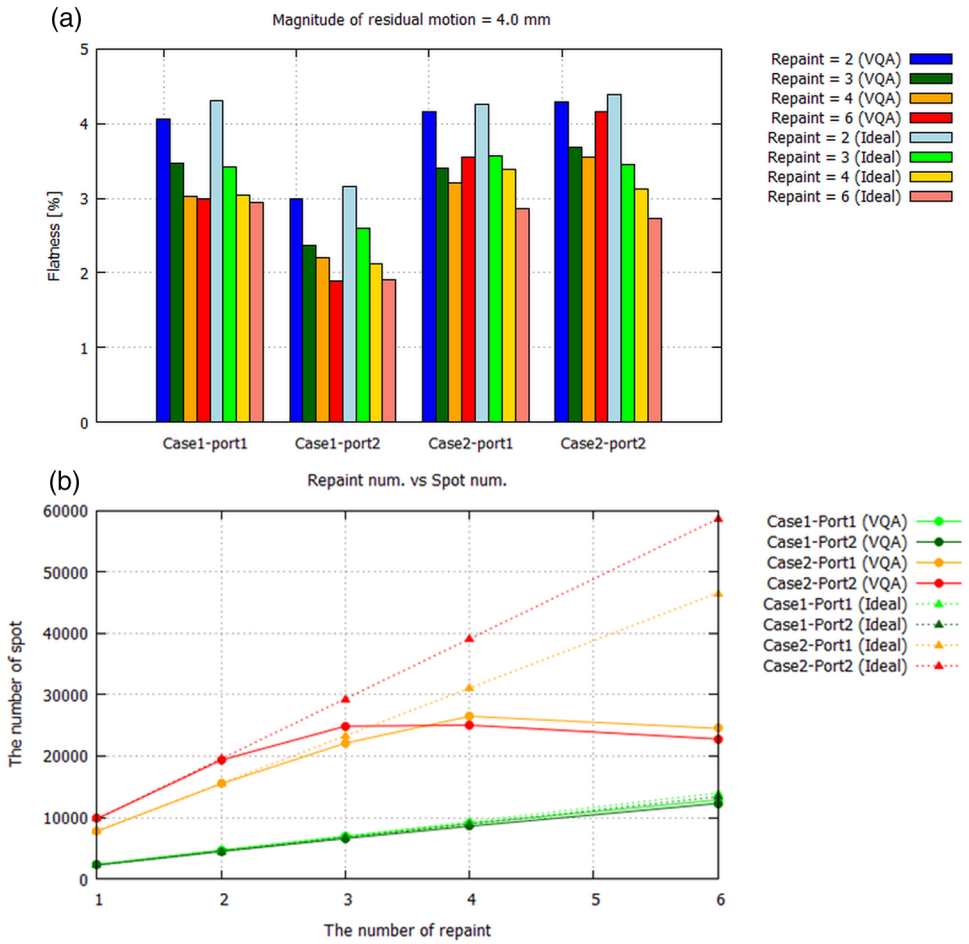


**FIGURE 8** (a) Flatness results for both ports of liver cases (Cases 1 and 2) when the magnitude of residual motion was 4.0 mm. Each box shows the result of flatness for each number of repaint (Repaint = 2, 3, 4, and 6). One method of repainting was based on the treatment-planning system (VQA) and the other was to repeat all spots completely with the set repainting number (ideal). (b) The relation between the number of repaints and the total number of spots for each port. The solid lines with circles indicate the results obtained using VQA repainting (VQA), and the dashed lines with triangles represent those obtained with ideal repainting (ideal)

## 4 | DISCUSSION

For the commissioning of the respiratory-gated CIRT at Osaka-HIMAK, we performed several types of measurements and simulations. In brief, the flatness and gamma passing rate improved as the number of repaintings increased in both the measurements and the simulations. We assume that the uniformity of the dose distribution for a moving target becomes robust when using a repainting method, as demonstrated by Phillips et al.[9]

From the results of our measurements, the gamma passing rates exceeded 95%, including the error bars, if the magnitude of the residual motion was less than 5.0 mm and the number of repaintings was more than 3. Except for the four paintings in the case of residual motion with magnitude 7.0 mm, the gamma passing rates exceeded 95%, including the error bars with more than three paintings. The magnitude of residual motion is recommended by AAPM TG-76 (<5.0 mm).[17] Although EPTN recommends the use of techniques such as rescanning to mitigate the motion effect, it does not indicate the specific number.[25] Therefore, the effectiveness of rescanning should be evaluated on a facility and patient-specific basis owing to inherent or mandatory rescanning requirements of system-specific parameters for the delivery systems.[19] Based on these results and TG-76, we chose the magnitude of the residual motions to be less than 5.0 mm and the number of repaintings to be more than 3.

Further, we performed simulations of respiratory-gated CIRT. Using the simple irradiation pattern, both the flatness and gamma passing rate improved as the number of repaintings increased. The criteria for the gamma passing rates were 2%/2 mm, which were stricter criteria than those normally used in patient-specific quality assurance at our facility. If the number of repaintings was greater than 3 and the size of the residual vibrations was less than 3.0 mm, the gamma passing rate exceeded 95%. The flatness results were around 3.0% if the magnitude of the residual motions was less than 2.0 mm and the number of repaintings was greater than 4. A similar trend was observed for the results using the simple irradiation pattern for the actual liver instances with both the VQA and the ideal repainting procedure if the number of repaintings was less than 4. The flatness results for almost all ports were less than 3.0% if the magnitude of the residual motions was less than 3.0 mm and the number of repaintings was 4 for both the repainting algorithms. This was similar to the magnitude criterion derived via the simulation using the simple irradiation pattern. Considering these results and the treatment time, we chose the basic number of repaintings to be 4 and the magnitude of the residual motions to be 3.0 mm.

However, the flatness results for the VQA repainting algorithm became worse when the number of repaintings was more than 4 if the prescribed dose was 60 Gy(RBE)/12 fx (Case 2). These results correspond to the relation between the number of repaintings and the total number of spots, which deviates greatly from a linear relationship. Unfortunately, with current specifications, the number of repaintings set by treatment planners is considered only after the completion of the optimization process using the VQA repainting algorithm. When some spots have small MU values that cannot be divided by the set number of repaintings owing to the limitation that the minimum MU/spot is 0.0016 MU, the number of repaintings of these spots is forced to be set to 1. In Case 2, we estimate that the MU of each spot became smaller relative to that in Case 1. Therefore, in Case 2, may be many spots that were created did not satisfy the number of repaintings set by the planner and the flatness was not improved, although the repaint number was increased.

A number of methods can be considered to avoid the abovementioned problem. In the opinion of treatment planners, the ideal solution would be to consider the number of repaintings during treatment planning for the optimization process. One method for incorporating the number of repaintings into the optimization process would be to include a penalty term for ensuring that MU/spot values are as uniform as possible. Another method would be to remove spots with small MU values and modify the MU values of the remaining spots during optimization.

A simple conceivable solution that does not change the optimization algorithm would be to set the minimum MU/spot in the optimization process to MU/spot values that can be divided by the given number of repaintings (e.g., set the minimum MU/spot value in the optimization process to 0.0096 MU if the number repaintings is set to 6). In the current specifications, because planners can change only the minimum MU/spot value to the limiting value derived from the treatment machine, the minimum MU/spot value for dividing each MU/spot value with set repaint number is changed to be the same as the spot value. (e.g., when planners change this value from 0.0016 to 0.0032 MU, the minimum MU/spot value for dividing each spot MU value by repainting number is also changed to 0.0032 MU). However, a concern with this simple method is that the flatness of the dose distribution becomes worse if the number of repaintings is set to large number.

Using ideal repainting, the flatness results in the liver cases fell within ~3.0%, even if the magnitude of residual motion was 5.0 mm. If the VQA repainting algorithm was improved and the number of repaintings was set to 6, the magnitude of the residual motions could be increased, which would contribute to reducing the treatment time.

As another approach, it was indicated by Richter et al. that the robustness for moving target can be improved by increasing the spot size.[26] This method is advantageous as compared with repainting when the treatment

time should not be prolonged. Although we could not study about the method of spot size increasing in detail because the beam size of our facility is fixed, the method is considerable to be introduced in our system or combined with decreased repainting.

In proton therapy facilities, adaptive radiation therapy was performed using 4D CBCT.[27] Many carbon-ion therapy facilities do not have gantry and it is considerable to use the in-room CT. Our facility installed an in-room CT to the second treatment room and it was useful for patient positioning and dose evaluations. However, the system was not arranged for adaptive radiation therapy owing to problems such as considerable time consumption for replanning. We will resolve this problem as a future task.

Finally, the methodological limitations of this study are described as follows. In the simulation of this study, 4D parameters such as scan speed and spill time were summarized to the probability-density function of spot position derived from the respiration motion. By improving the VQA via the introduction of the probability-density function to import deformation information or export linear energy transfer distribution, it is expected to perform more detailed simulation like 4DTPS, as indicated by Richter et al.[28] Moreover, the limited conditions of the experiment and simulation owing to the time constraints were one of the limitations and it can be resolved by increasing the types of ports or parts of treatment.

## 5 | CONCLUSIONS

Our facility began the respiratory-gated CIRT in November 2018, and some measurements and simulations were performed to determine the treatment conditions during commissioning. Although some features are not provided or are different at our facility as compared with other leading facilities, we conclude that our approaches can provide sufficiently precise treatment. With improvements in the VQA repainting algorithm, we expect the treatments at our facility to improve for moving targets.

### ACKNOWLEDGMENTS

We would like to thank to all the doctors in Osaka-HIMAK for their support and discussions for making treatment plans, the QA committee in Osaka-HIMAK for their meaningful discussions on the commissioning, and the members of Osaka Heavy-Ion Administration Company for their support regarding the measurements. Masaaki Takashina would like to thank JSPS KAKENHI for the financial support; Grant Number JP17H04119.

### CONFLICT OF INTEREST

The authors declare no conflict of interest.

### DATA AVAILABILITY STATEMENT

Research data are not shared.

### REFERENCES

1. Suit H, DeLaney T, Goldberg S, et al. Proton vs carbon ion beams in the definitive radiation treatment of cancer patients. *Radiother Oncol*. 2010;95(1):3-22.
2. Inaniwa T, Furukawa T, Kanematsu N, et al. Evaluation of hybrid depth scanning for carbon-ion radiotherapy. *Med Phys*. 2012;39(5):2820-2825.
3. Bert C, Rietzel E. 4D treatment planning for scanned ion beams. *Radiat Oncol*. 2007;2:24.
4. Bert C, Grözinger SO, Rietzel E. Quantification of interplay effects of scanned particle beams and moving targets. *Phys Med Biol*. 2008;53(9):2253-2265.
5. Chui CS, Yorke E, Hong L. The effects of intra-fraction organ motion on the delivery of intensity-modulated field with a multileaf collimator. *Med Phys*. 2003;30(7):1736-1746.
6. Grözinger SO, Bert C, Haberer T, Kraft G, Rietzel E. Motion compensation with a scanned ion beam: a technical feasibility study. *Radiat Oncol*. 2008;3(1):34.
7. Grözinger SO, Rietzel E, Li Q, Bert C, Haberer T, Kraft G. Simulations to design an online motion compensation system for scanned particle beams. *Phys Med Biol*. 2006;51(14):3517-3531.
8. Furukawa T, Inaniwa T, Sato S, et al. Moving target irradiation with fast rescanning and gating in particle therapy. *Med Phys*. 2010;37(9):4874-4879.
9. Phillips MH, Pedroni E, Blattmann H, Boehringer T, Coray A, Scheib S. Effects of respiratory motion on dose uniformity with a charged particle scanning method. *Phys Med Biol*. 1992;37(1):223-234.
10. Mizuno H, Saito O, Tajiri M, et al. Commissioning of a respiratory gating system involving a pressure sensor in carbon-ion scanning radiotherapy. *J Appl Clin Med Phys*. 2019;20(1):37-42.
11. Shimizu S, Miyamoto N, Matsuura T, et al. A proton beam therapy system dedicated to spot-scanning increases accuracy with moving tumors by real-time imaging and gating and reduces equipment size. *PLOS ONE*. 2014;9(4):e94971.
12. Mori S, Inaniwa T, Furukawa T, et al. Amplitude-based gated phase-controlled rescanning in carbon-ion scanning beam treatment planning under irregular breathing conditions using lung and liver 4DCTs. *J Radiat Res*. 2014;55(5):948-958.
13. Takahashi W, Mori S, Nakajima M, et al. Carbon-ion scanning lung treatment planning with respiratory-gated phase-controlled rescanning: simulation study using 4-dimensional CT data. *Radiat Oncol*. 2014;9:238.
14. Mori S, Inaniwa T, Furukawa T, Zenklusen S, Shirai T, Noda K. Effects of a difference in respiratory cycle between treatment planning and irradiation for phase-controlled rescanning and carbon pencil beam scanning. *Br J Radiol*. 2013;86(1028):20130163.
15. Herfarth KK, Debus J, Lohr F, et al. Extracranial stereotactic radiation therapy: set-up accuracy of patients treated for liver metastases. *Int J Radiat Oncol Biol Phys*. 2000;46(2):329-335.
16. Fattori G, Seregni M, Pella A, et al. Real-time optical tracking for motion compensated irradiation with scanned particle beams at CNAO. *Nucl Instrum Methods Phys Res A*. 2016;827:39-45.
17. Paul JK, Gig SM, James MB, et al. The management of respiratory motion in radiation oncology report of AAPM Task Group 76. *Med Phys*. 2006;33(10):3874-3900.
18. Katarzyna C, Frank E, Renata K, et al. Clinical practice vs. state-of-the-art research and future visions: report on the 4D treatment planning workshop for particle therapy – edition 2018 and 2019. *Phys Med*. 2021;82:54-63.
19. Chang JY, Zhang X, Knopf A, et al. Consensus guidelines for implementing pencil-beam scanning proton therapy for thoracic malignancies on behalf of the PTCOG Thoracic and Lymphoma Subcommittee. *Int J Radiat Oncol Biol Phys*. 2017;99(1):41-50.
20. Miriam K, Grischa K, Giovanni F, et al. Experimental validation of a deforming grid 4D dose calculation for PBS proton therapy. *Phys Med Biol*. 2018;63(5):055005.

21. Rodríguez-Molinero A, Narvaiza L, Ruiz J, Gálvez-Barrón C. Normal respiratory rate and peripheral blood oxygen saturation in the elderly population. *J Am Geriatr Soc*. 2013;61(12):2238-2240.
22. Low DA, Harms WB, Mutic S, Purdy JA. A technique for the quantitative evaluation of dose distributions. *Med Phys*. 1998;25(5):656-661.
23. Benchetrit G. Breathing pattern in humans: diversity and individuality. *Respir Physiol*. 2000;122(2-3):123-129.
24. Hossain M, Rhoades J. On beam quality and flatness of radiotherapy megavoltage photon beams. *Australas Phys Eng Sci Med*. 2016;39(1):135-145.
25. ESTRO The WP5 collective PTPS specifications. https://www.estro.org/ESTRO/media/ESTRO/Science/WP5-Collective-PTPS-specifications-rebranded.pdf. September the 22th, 2021.
26. Richter D, Graeff C, Jäkel O, et al. Residual motion mitigation in scanned carbon ion beam therapy of liver tumors using enlarged pencil beam overlap. *Radiother Oncol*. 2014;113(2):290-295.
27. Trnková P, Knäuslc B, Actisd O, et al. Clinical implementations of 4D pencil beam scanned particle therapy: report on the 4D treatment planning workshop 2016 and 2017. *PhysMed*. 2018;54:121-130.
28. Richter D, Schwarzkopf A, Trautmann J, et al. Upgrade and benchmarking of a 4D treatment planning system for scanned ion beam therapy. *Med Phys*. 2013;40(5):051722.

**How to cite this article:** Hamatani N, Tsubouchi T, Takashina M, Yagi M, Kanai T. Commissioning of carbon-ion radiotherapy for moving targets at the Osaka Heavy-Ion Therapy Center. *Med Phys*. 2022;49:801–812.
https://doi.org/10.1002/mp.15403